Available online at www.sciencedirect.com
SCIENCE DIRECT®
Advances in Water Resources 26 (2003) 1041–1060
Advances in Water Resources
www.elsevier.com/locate/advwatres

A coupled local–global upscaling approach for simulating flow in highly heterogeneous formations

Y. Chen [a], L.J. Durlofsky [a,b,*], M. Gerritsen [a], X.H. Wen [b]

[a] Department of Petroleum Engineering, Stanford University, Green Earth Sciences Building, Stanford, CA 94305-2220, USA
[b] Chevron Texaco Exploration & Production Technology Company, San Ramon, CA 94583-0719, USA

Received 28 January 2003; received in revised form 8 July 2003; accepted 9 July 2003

Abstract

A new technique for generating coarse scale models of highly heterogeneous subsurface formations is developed and applied. The method uses generic global coarse scale simulations to determine the boundary conditions for the local calculation of upscaled properties (permeability or transmissibility). An iteration procedure assures consistency between the local and global calculations. Transport processes are simulated using a subgrid velocity reconstruction technique applied in conjunction with the local–global upscaling procedure. For highly heterogeneous (e.g., channelized) systems, the new method is shown to provide considerably more accurate coarse scale models for flow and transport, relative to reference fine scale results, than do existing local (and extended local) upscaling techniques. The applicability of the upscaled models for different global boundary conditions is also considered.

Keywords: Scale up; Subsurface; Heterogeneity; Flow simulation; Subgrid; Transport; Channelized; Permeability; Transmissibility

1. Introduction

Subsurface formations typically display high degrees of variability over multiple length scales. Rock properties such as permeability are in many cases best described by multi-point geostatistical characterizations. Such systems may exhibit geometrically complex features with complicated large scale connectivity. This permeability variability and complex connectivity fundamentally impact subsurface flow and transport behavior. For this reason these effects must be included in simulations of realistic aquifers or petroleum reservoirs.

The effects of subsurface heterogeneity can be included either through the solution of stochastic flow equations or by simulating a number of geostatistical realizations. In this latter approach, which is the framework applied here, each particular realization is viewed as deterministic. In order to obtain useful flow and transport results with such systems, it is essential that the models include geologically realistic subsurface characterizations. This greatly impacts computational requirements, as the direct simulation of flow in highly resolved multiscale systems is very demanding.

Upscaling techniques are often introduced to coarsen these geological models to manageable levels for flow calculations. It is important that these coarsened flow models replicate the fine scale characterizations in terms of key behaviors such as overall flow rate (for given boundary conditions or well pressures) and the appearance of injected fluid or pollutant at a particular location or well. For subsurface systems that can be represented by two-point geostatistics (e.g., spherical or exponential variogram models), a number of coarsening techniques (as indicated below) have been developed and successfully applied. For the highly heterogeneous systems addressed in this paper, however, the upscaling methods that perform adequately for the simpler geostatistical models are observed to fail in many cases.

Upscaling techniques can be characterized as local, extended local, global or quasi-global, depending on the size of the region used for the calculation of the coarse scale quantities. A number of upscaling procedures are discussed in earlier reviews [1–3] and in papers comparing the performance of the various techniques (e.g., [4] for power averaging techniques and [5] for numerical flow-based methods). In purely local approaches (e.g., [5–7]), the upscaled parameters are computed over fine

* Corresponding author. Address: Department of Petroleum Engineering, Stanford University, Green Earth Sciences Building, Stanford, CA 94305-2220, USA. Tel.: +1-650-723-4142; fax: +1-650-725-2099.
E-mail address: lou@pangea.stanford.edu (L.J. Durlofsky).

0309-1708/$ - see front matter © 2003 Elsevier Ltd. All rights reserved.
doi:10.1016/S0309-1708(03)00101-5

scale regions corresponding only to the target coarse block under study. In extended local procedures (e.g., [8–12]), fine scale information from neighboring regions is also used in the upscaling calculations. Global methods, by contrast, utilize global fine scale flow simulations for the determination of coarse scale parameters [13–16]. Quasi-global approaches reduce the computational requirements of full global procedures by substituting some type of approximate global information in place of global fine scale results. Most previous upscaling procedures are directed toward the computation of coarse scale permeability, though a number also consider the calculation of upscaled transmissibility (e.g., [13–16]).

In this paper we develop and apply a novel coupled local–global upscaling technique for application to highly heterogeneous geostatistical realizations. The method differs from previous approaches in that the coarse scale parameters (upscaled permeability or transmissibility) are computed iteratively using local boundary conditions determined from global coarse scale single-phase flow solutions. This coupled local–global upscaling procedure can be classified as a quasi-global approach. The method requires more computation than existing extended local upscaling procedures though it does not require any global fine scale flow simulations. The upscaling technique is combined with a subgrid velocity reconstruction procedure [17] for transport calculations. Coarse scale predictions for flow and transport using the new method are shown to be considerably more accurate than are those using existing extended local upscaling techniques.

Our local–global upscaling technique shares some similarities with previous "dual-grid" procedures (e.g., [17–19]) and adaptive mesh refinement techniques. Dual-grid methods provide fine grid approximations from global coarse grid solutions. Our method differs from these approaches in that our emphasis is on the determination of upscaled quantities for use in subsequent simulations. The local–global approach is also related to multigrid upscaling [20]. In contrast to this approach, however, our method does not require any global fine scale calculations. In addition, we consider two complementary generic global flow problems (rather than one specific global flow simulation) in our determination of the coarse scale parameters.

In the current work, we apply the velocity reconstruction technique presented in [17]. This method allows for the generation of an approximate fine scale velocity field that is consistent (in terms of integrated flow through regions corresponding to coarse block edges) with the global coarse solution. Dual-grid and velocity reconstruction techniques are also related to multiscale modeling procedures (e.g., [21,22] in the context of finite element methods and [23] for a full tensor flux-continuous finite volume approach), in which the base functions, formed using subgrid permeability information, are subsequently employed to reconstruct the fine scale velocity. A novel aspect of our method lies in the iterative coupling between local and global flows. Applying this approach, we demonstrate improved accuracy in both coarse scale properties and fine scale reconstructions.

This paper proceeds as follows. We first present the flow and transport equations and the finite difference numerical scheme for solving the flow equation. The potential limitations of the local boundary conditions applied in standard upscaling methods are then demonstrated. The new coupled local–global upscaling procedure and the solution of the transport equation are described in detail in Section 3. Flow results for two-dimensional models, in terms of total flow through the system, are presented in Section 4. In Section 5 we present transport calculations using the coupled upscaling approach in conjunction with the reconstruction of subgrid velocity. We then discuss potential enhancements to the method and finally present our conclusions.

2. Governing equations and local boundary conditions

In this section, we present the equations governing flow and transport for a unit mobility ratio displacement. This system is identical to that used to describe purely advective pollutant transport or the transport of a passive scalar. We then motivate the coupled local–global upscaling approach by considering the local pressure field over a coarse block region obtained from a global fine scale simulation.

2.1. Fine and coarse scale equations

The dimensionless pressure equation governing steady state, incompressible, single-phase flow is obtained by combining the continuity equation ($\nabla \cdot \mathbf{u} = 0$) and Darcy's law ($\mathbf{u} = -\mathbf{k} \cdot \nabla p$)

$$\nabla \cdot (\mathbf{k} \cdot \nabla p) = 0. \tag{1}$$

Here p is dimensionless pressure, $\mathbf{u}$ is Darcy velocity and $\mathbf{k}$ is the permeability tensor, which is in general highly variable in space (note that all quantities are dimensionless; permeability is non-dimensionalized by a reference or characteristic permeability). For a unit mobility ratio displacement, in which the displacing fluid has identical properties to those of the displaced fluid, the transport equation with capillary pressure and gravity neglected is given by:

$$\frac{\partial S}{\partial t} + \nabla \cdot (\mathbf{u}S) = 0, \tag{2}$$

where S is the saturation (volume fraction) of the displacing fluid and t is time. Note that for a unit mobility

ratio displacement, changes in saturation have no effect on pressure; i.e., Eqs. (1) and (2) are decoupled.

Eqs. (1) and (2) describe flow and transport on the fine scale. The intent of upscaling is to generate appropriate coarse properties and/or procedures to solve flow and transport on the coarse scale while maintaining important aspects of the fine scale behavior. The homogenization of equations with variable coefficients often yields coarse scale equations of a different form than the original fine scale equations. When scale separation exists, it has been shown in [24] that the coarse scale pressure equation is of the same form as the fine scale equation but with the permeability $\mathbf{k}$ replaced by the coarse scale or effective permeability tensor $\mathbf{k}^*$. In more general cases in which there is no separation of scales, numerical results in a variety of contexts (e.g., [5,7]) have demonstrated that the coarse system can still be described in terms of an upscaled equivalent permeability tensor $\mathbf{k}^*$. Therefore, as is common practice, in this work we take the coarse scale pressure equation to be of the same form as Eq. (1), but with $\mathbf{k}$ replaced by $\mathbf{k}^*$:

$$\nabla \cdot (\mathbf{k}^* \cdot \nabla p^c) = 0, \tag{3}$$

where p^c designates pressure on the coarse scale. In this work the transport equation is solved on the fine scale with $\mathbf{u}$ in Eq. (2) reconstructed using local flow solutions, so there is no need to consider the coarse scale analog of Eq. (2).

A finite difference discretization is applied for the numerical solutions of the fine and coarse scale pressure equations. We present the discretization and methodology for a two-dimensional system. Extension to three dimensions is straightforward. Fig. 1a displays a fine grid (finer lines) and a corresponding coarse grid (heavier lines). Grid blocks are indexed by i in the x-direction and by j in the y-direction. For diagonal permeability tensors, the flow from block (i,j) to block $(i+1,j)$ depends only on the pressures in blocks (i,j) and $(i+1,j)$. A two-point flux calculation is therefore appropriate. This leads to the standard five-point stencil for the pressure equation:

$$\begin{aligned}&(T_x)_{i-1/2,j}(p_{i-1,j}-p_{i,j})+(T_x)_{i+1/2,j}(p_{i+1,j}-p_{i,j})\\&\quad+(T_y)_{i,j-1/2}(p_{i,j-1}-p_{i,j})+(T_y)_{i,j+1/2}(p_{i,j+1}-p_{i,j})=0,\end{aligned} \tag{4}$$

where $p_{i,j}$ designates pressure in grid block (i,j) and $(T_x)_{i\pm1/2,j}$ and $(T_y)_{i,j\pm1/2}$ are interblock transmissibilities in the x and y directions. The transmissibility in x between blocks (i,j) and $(i+1,j)$ is defined as:

$$(T_x)_{i+1/2,j}=\frac{2(k_x)_{i+1/2,j}\Delta y_j h}{\Delta x_{i+1}+\Delta x_i}. \tag{5}$$

Here h is the model thickness and Δx_i and Δy_j denote the dimensions of grid block (i,j). The interface permeability $(k_x)_{i+1/2,j}$ is calculated via the harmonic average of the block permeabilities $(k_x)_{i,j}$ and $(k_x)_{i+1,j}$:

$$(k_x)_{i+1/2,j}=\frac{(\Delta x_i+\Delta x_{i+1})(k_x)_{i,j}(k_x)_{i+1,j}}{\Delta x_{i+1}(k_x)_{i,j}+\Delta x_i(k_x)_{i+1,j}}. \tag{6}$$

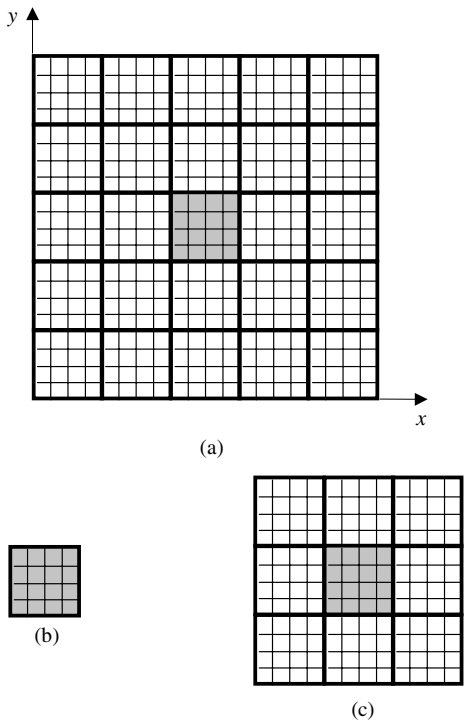

Fig. 1. Schematic showing (a) fine and coarse scale grids, (b) fine scale local region and (c) fine scale extended local region ($r=1$).

Transmissibilities and interface permeabilities in the y-direction are defined analogously. The above discretization scheme can be also applied to the coarse scale pressure equation, assuming the two-point flux calculation is applicable.

If the permeability is a full tensor, the two-point flux calculation must be replaced by a multi-point flux calculation, which will give a more complex (nine-point) finite difference stencil [25]. In this work, the fine scale permeability is isotropic. On the coarse scale, an anisotropic full tensor is obtained if permeability upscaling is performed. In this case, we apply a multi-point flux continuous finite difference scheme (e.g., [25]) to solve the coarse scale pressure equation. It is also possible to compute upscaled transmissibility T_x^* and T_y^* directly from the extended local flow problems (as will be discussed below). For transmissibility upscaling, only two-point flux calculations are considered in this work. The numerical results in Section 4 show that the two-point flux calculation with transmissibility upscaling can provide accurate coarse models for the cases considered. The transmissibility upscaling could in principle be extended to handle multi-point fluxes using a variant of the approach presented in [23].

2.2. Motivation for upscaling

The fine scale solution of Eqs. (1) and (2) can, in practical cases, be very demanding computationally. Specifically, detailed three-dimensional geocellular models of the subsurface may contain $O(10^7$–$10^8)$ cells. Practical simulation models, by contrast, typically contain $O(10^5$–$10^6)$ grid blocks. Thus, an upscaling methodology that can provide a factor of 5–10 coarsening in each coordinate direction would be very useful in practice.

Although the upscaling techniques presented here do require some amount of computation, these calculations need only be performed once in a pre-processing step. The computational savings achieved using the upscaled model will be realized each time the model is run. In such cases, the computational requirements of local or extended local upscaling techniques (including iterated techniques as developed here) will be small relative to the cost of fine scale simulations. This assumes that the upscaled model is sufficiently robust to use for a number of flow scenarios. This issue will be discussed further in Sections 5 and 6.

Upscaling techniques developed for single-phase flow are also generally applicable for two-phase flow, in which case the pressure equation must be solved at each time step as the displacement evolves (due to relative permeability effects). In this case, even if only one flow scenario is to be simulated, the computational savings using the upscaled model will be very significant. For example, in previous work using flow-based grid generation and an extended local upscaling procedure, the (two-dimensional) coarse model ran 60 times faster than the fine grid model (with upscaling by a factor of five in each coordinate direction). The grid generation and upscaled property calculations required only about 0.4% of the computation time of the fine scale simulation for that case [11]. The applicability of our upscaling procedure to a two-phase flow problem will be illustrated in Section 4.5. These examples demonstrate the potential savings offered by an accurate upscaling technique.

2.3. Boundary conditions for the local flow problem

Numerical flow-based upscaling often entails solving fine scale local flow in each coarse block. For a given coarse block (the shaded region in Fig. 1a), the local flow can be solved either purely locally (Fig. 1b) or in an extended local region (Fig. 1c). The latter case is also referred to as "border region upscaling," considered previously [8–12]. Following [12], we quantify the size of the border region in terms of the number of "bordering rings" of coarse cells that surround the target coarse block. This quantity is represented by r. If we set $r = 1$, this means that we solve over a fine scale region corresponding to the target coarse block plus one ring of coarse blocks, as shown in Fig. 1c.

In any type of local or extended local upscaling technique, boundary conditions on the local problem must be specified in order for the coarse scale equivalent permeability or transmissibility to be computed. A number of boundary specifications are used in practice (e.g., pressure—no flow, periodicity, linear pressure), though they are generally based on the assumption of a locally constant pressure difference over the local region. For a two-dimensional problem, Eq. (1) must be solved twice over the local (or extended local) fine scale region in order to obtain all of the required components of the upscaled permeability or transmissibility. We consider a local flow on a region of physical dimensions $l_x \times l_y$. For constant pressure—no flow boundary conditions, we first solve the local problem subject to:

$$\begin{aligned} &p(0,y) = 1, \\ &p(l_x,y) = 0, \\ &u_y(x,0) = u_y(x,l_y) = 0. \end{aligned} \tag{7}$$

Local flow driven by a pressure difference in the y-direction is then solved. Other commonly used boundary conditions, such as periodicity [7,12,26], also assume a constant pressure difference over the local domain.

The choice of local boundary conditions is an important issue in numerical upscaling methods. In some cases, the local boundary conditions may have a strong impact on the accuracy of flow results. In order to assess the applicability of these assumed local boundary conditions, we now perform global fine scale simulations and extract the fine scale pressures over regions corresponding to the boundaries of coarse blocks. By comparing these "actual boundary conditions" with the assumed boundary conditions, we can gauge the accuracy of the local boundary specifications.

We consider fine and coarse scale systems that are 100×100 and 10×10 grid blocks respectively (this corresponds to a factor of 10 upscaling in each direction). Fig. 2 shows the permeability distribution and the difference in pressure across the fine scale region (10×10 blocks) corresponding to a single coarse block for layered and channelized systems (the large scale layers and channels are not apparent in the regions shown in Fig. 2). With the global flow in the y-direction, the pressure difference in y between the top and bottom edges of the coarse block region is plotted against the fine grid locations in x. The dashed line in Fig. 2b and d represents the mean value of $|\Delta p|$. We see that the pressure difference is not a constant even for the layered system (Fig. 2b), though in this case it varies by less than a factor of two. There is considerably more variation in the case of the highly heterogeneous channelized system (Fig. 2d), where $|\Delta p|$ varies by almost an order of magnitude. These two examples illustrate that the actual pressure

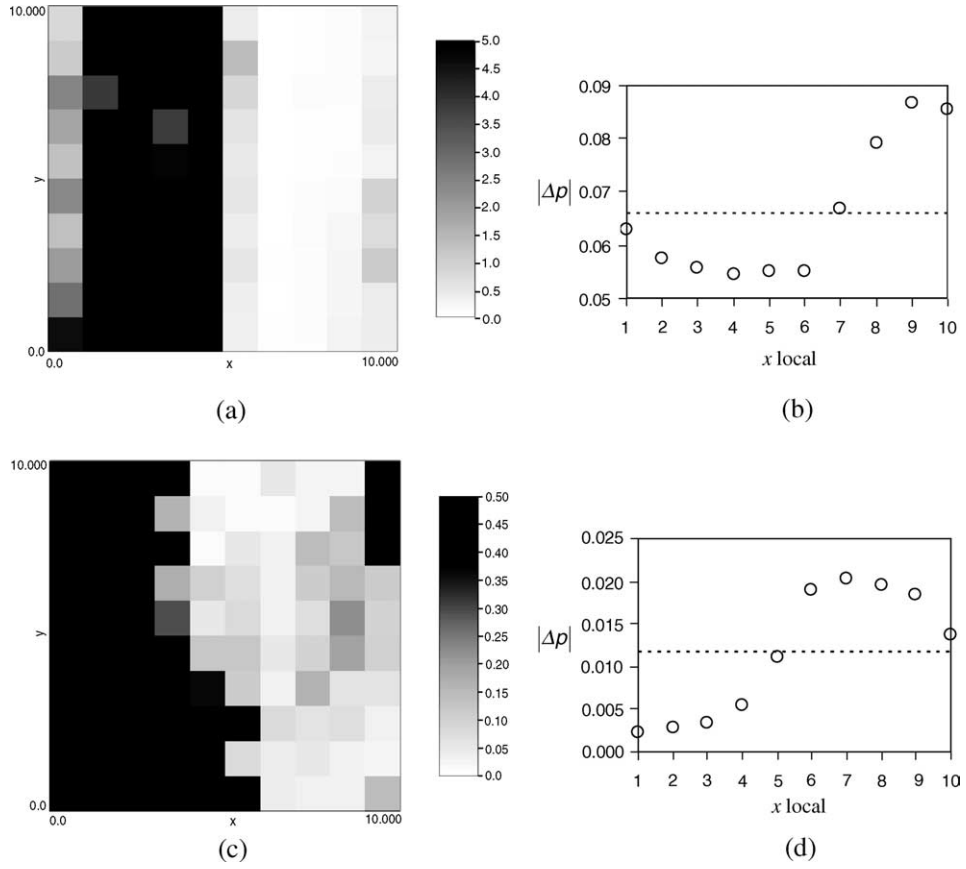

Fig. 2. Pressure difference over a single coarse block from global fine scale solutions: (a) permeability for layered system, (b) pressure difference for layered system, (c) permeability for channel system and (d) pressure difference for channel system.

difference over the coarse block region can deviate significantly from a constant. This variation is affected by both the global boundary conditions and the subgrid heterogeneities. These results provide the motivation for our coupled procedure, which computes the upscaled properties using boundary conditions determined from the global flow field, as we describe in the next section.

We note that our method is related in concept to the use of effective flux boundary conditions for the upscaling of relative permeabilities [27]. The intent of these boundary conditions is to adjust the local pressure difference based on the magnitude of the local fine scale permeability relative to the average global background permeability. This acts to capture the interaction of local and global effects in the calculation of the upscaled relative permeabilities. Effective flux boundary conditions are not directly applicable for our calculations here, however, since we do not observe a clear scaling of $|\Delta p|$ with the local permeability in highly heterogeneous channelized systems (as was observed in the more continuous permeability fields considered in [27]). In addition, we are interested here in upscaled single-phase properties, in contrast to the upscaled relative permeabilities computed in [27].

3. Coupled local–global upscaling procedure

In the coupled local–global upscaling method, we directly use global flow information to adjust the local boundary conditions used in the calculation of upscaled properties. By global flow here, we mean two generic global flows (i.e., large scale flows in the x and y directions). The upscaled permeabilities or transmissibilities are then recomputed from the local flow problems and the global flow is solved again. This procedure is iterated until the global flow and the upscaled properties are consistent, at which point the system has converged to a self-consistent solution. For the first iteration, an existing upscaling technique is applied.

3.1. Determination of local boundary conditions from coarse scale global flow

A schematic illustrating the incorporation of the global coarse pressure into the local boundary conditions is presented in Fig. 3. Coarse pressures are determined from the coarse scale solution on the global domain, shown in the left plot of Fig. 3. Displayed in the right plot is the extended local region we use for the calculation of coarse properties, where a border region

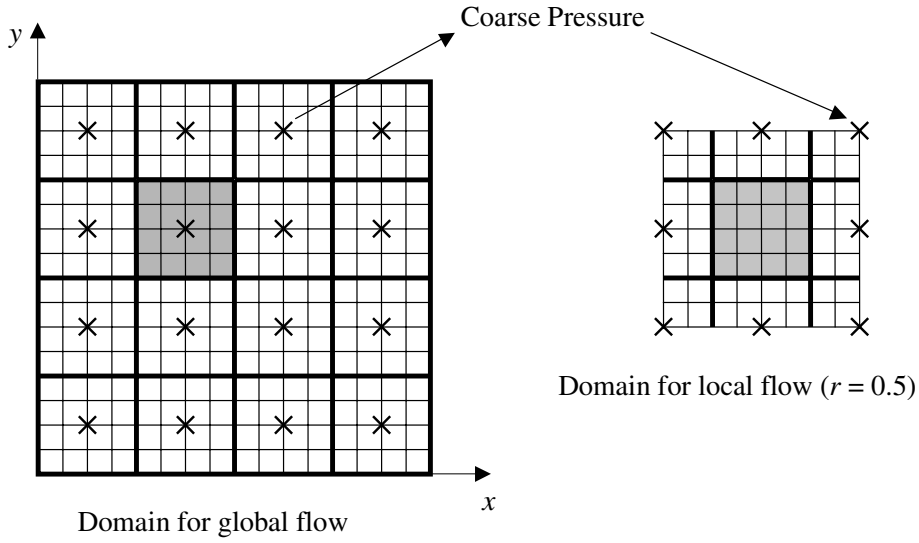

Fig. 3. Schematic showing coupling of global coarse scale pressure into local fine scale flow calculations.

with $r = 0.5$ is illustrated (the target cell is shaded). The choice of the "half" ring makes it straightforward to transfer the coarse pressure on the global coarse grid (designated by ×'s in Fig. 3) to the local fine scale grid. Analogously, we may also apply coarse pressures on the boundaries of a larger region; e.g., $r = 1.5$. Coarse pressure values obtained from global coarse solutions are assigned to the corresponding local boundary locations and interpolation (described below) is performed to define pressures for the other fine scale boundary locations.

Previous local and extended local upscaling techniques require that Eq. (1) be solved twice (for two-dimensional problems) over the local region, once with flow driven in the x-direction and once with flow in the y-direction. Similarly, here we also require the solution of two flow problems over the extended local region. Since the local boundary conditions are determined from the global flow, two global flow problems must also be solved. These global flow problems could be specified in a number of different ways. The approach taken here is to specify large scale flows that are nominally in the x and y directions respectively. These flows, which we refer to as "generic global flows," are obtained by fixing (different) constant pressures on two opposite boundaries and no-flow conditions on the other two boundaries. This global specification provides local flows that have relatively strong x and y components, which in turn allows for the accurate calculation of upscaled quantities. We note that other global flows could also be specified, though we have found that the specification used here provides coarse scale descriptions that are in many cases applicable for use with other global boundary conditions. In a later paper, we will describe the extension of the method to more general global flows; i.e., coarse scale properties are computed from general flows driven by wells.

We now describe the interpolation scheme used to obtain pressures at local fine scale boundaries, as required for the calculation of $\mathbf{k}^*$ or T^*. For the local problem, we consider a computational domain of size $l_x \times l_y$ discretized by $n_x \times n_y$ blocks with grid block size $\Delta x_i \times \Delta y_j$, as shown in the right plot of Fig. 3 (here $n_x = n_y = 8$). The blocks along the bottom boundary ($y = 0$) of this extended local region are plotted in Fig. 4. Again, ×'s designate pressures computed from the global coarse flows. The solid circles in Fig. 4 designate local fine scale boundary pressures, which are required on the block edges.

Two procedures, linear and harmonic interpolations, will be applied to determine the local boundary pressures. Coarse pressures p_1^c and p_2^c are known at locations x_1^c and x_2^c. To determine the fine scale pressures $p_{i,0}$ via linear interpolation, we apply

$$p_{i,0} = p_1^c + (x_i - x_1^c)\frac{p_2^c - p_1^c}{x_2^c - x_1^c}, \quad x_1^c < x_i < x_2^c, \tag{8}$$

where x_i is the fine grid location. Similarly, coarse pressures p_2^c and p_3^c can be interpolated to obtain $p_{i,0}$ for $x_2^c < x_i < x_3^c$.

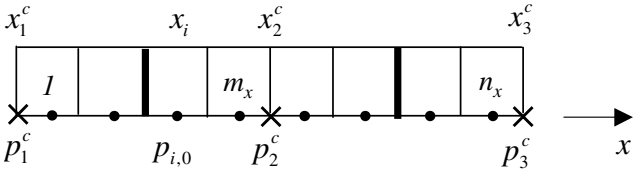

Fig. 4. Schematic showing interpolation of pressure at local fine scale boundary ($y = 0$).

For harmonic interpolation, weightings based on the fine scale permeabilities of the boundary blocks are applied. Pressures are obtained by considering one-dimensional flow along a series of heterogeneous blocks. Specifically, the fine scale boundary pressures for $x_1^c < x_i < x_2^c$ are obtained via:

$$p_{i,0} = p_1^c + (x_i - x_1^c)\frac{p_2^c - p_1^c}{x_2^c - x_1^c}\frac{k^h}{k_i^h}, \quad x_1^c < x_i < x_2^c, \tag{9}$$

where k^h is the effective permeability defined as the weighted harmonic average of the individual block permeabilities (k_i) between x_1^c and x_2^c:

$$k^h = \frac{\sum_{i=1}^{m_x} \Delta x_i}{\sum_{i=1}^{m_x} \frac{\Delta x_i}{k_i}}. \tag{10}$$

Similarly, k_i^h is calculated using block permeabilities between x_1^c and x_i. An analogous procedure is applied for $x_2^c < x_i < x_3^c$.

In our method, two generic global flows are employed to determine the upscaled parameters. We apply harmonic interpolation of pressure in the main flow direction and linear interpolation in the secondary flow direction. Specifically, for global flow in the x-direction, which is used for the calculation of the x components of the upscaled properties, linear interpolation is applied in y along the boundaries $x = 0$ and $x = l_x$, while harmonic interpolation is used in x along $y = 0$ and $y = l_y$. When global flow is in y, by contrast, we apply linear interpolation along $y = 0$ and $y = l_y$ and harmonic interpolation along $x = 0$ and $x = l_x$.

This treatment is appropriate if we view the flow along the boundaries as locally one-dimensional. In limited tests, this approach was found to provide slightly more accurate upscaled models (in terms of their predictions for total flow through the system relative to fine scale models) than linear interpolation on all boundaries. It is of course possible that other interpolation schemes may improve accuracy even further. The key point to note is that, compared to the standard local boundary conditions, where constant pressure difference is assumed (Eq. (7)), the Dirichlet local boundary conditions applied here account for both the global flow effects and the subgrid heterogeneity.

3.2. Calculation of upscaled permeability or transmissibility

We now describe the procedures to calculate the upscaled $\mathbf{k}^*$ and T^* from the extended local problems and then comment on the differences between $\mathbf{k}^*$ upscaling and T^* upscaling for permeability fields with high variations.

Following the local fine scale solutions of Eq. (1) subject to the Dirichlet boundary conditions described above, we compute volume averages of $\mathbf{u}$ and ∇p over the target coarse block. The coarse scale Darcy's law $\langle \mathbf{u} \rangle = -\mathbf{k}^* \cdot \langle \nabla p \rangle$ is then inverted to obtain the four elements of $\mathbf{k}^*$:

$$\begin{aligned}
\langle u \rangle_x^1 &= -(k_{xx}^* \langle \nabla p \rangle_x^1 + k_{xy}^* \langle \nabla p \rangle_y^1),\\
\langle u \rangle_y^1 &= -(k_{yx}^* \langle \nabla p \rangle_x^1 + k_{yy}^* \langle \nabla p \rangle_y^1),\\
\langle u \rangle_x^2 &= -(k_{xx}^* \langle \nabla p \rangle_x^2 + k_{xy}^* \langle \nabla p \rangle_y^2),\\
\langle u \rangle_y^2 &= -(k_{yx}^* \langle \nabla p \rangle_x^2 + k_{yy}^* \langle \nabla p \rangle_y^2).
\end{aligned} \tag{11}$$

Here the subscript of $\langle u \rangle$ and $\langle \nabla p \rangle$ designates the vector component and the superscript the flow problem (1 corresponds to global flow in x and 2 to flow in y). From the two flow problems, the components of the full tensor $\mathbf{k}^*$ can be computed. In this work, we actually solve a least squares problem (Eq. (11) plus an additional equation of the form $k_{xy}^* - k_{yx}^* = 0$) to enforce the symmetry of $\mathbf{k}^*$ [12]. Potential problems with the positivity of upscaled properties will be discussed in Section 3.4. As mentioned in Section 2.1, a multi-point flux-continuous finite difference scheme [25] is applied to solve the coarse scale model described by the full tensor $\mathbf{k}^*$.

In some cases, it is advantageous to compute upscaled transmissibilities (T^*) directly rather than computing $\mathbf{k}^*$ and then using it to calculate T^*. Our formulation is quite general in this respect as the equivalent transmissibility across the interface between two coarse blocks can be readily computed from the local problem. In this work, for transmissibility upscaling we consider only two-point flux calculations, which is suitable for coarse scale models in which the cross terms of $\mathbf{k}^*$ are small relative to the diagonal terms, as is the case in many practical settings. For transmissibility upscaling in the context of multi-point flux calculations, refer to [23].

Under the assumption of two-point flux, transmissibility is calculated from the extended local solution using:

$$\begin{aligned}
(T_x^*)_{i+1/2,j} &= \frac{q_{i+1/2,j}^c}{\langle p \rangle_{i,j} - \langle p \rangle_{i+1,j}},\\
(T_y^*)_{i,j+1/2} &= \frac{q_{i,j+1/2}^c}{\langle p \rangle_{i,j} - \langle p \rangle_{i,j+1}},
\end{aligned} \tag{12}$$

where i and j are coarse block indices, T_x^* and T_y^* are the upscaled transmissibilities in the x and y directions, q^c is the total flow across the interface between adjacent coarse blocks (i.e., the sum of the fine grid flows over the region corresponding to the coarse block interface) and $\langle p \rangle$ is the volume average of the fine scale pressure over the coarse block.

Since transmissibility is defined at block interfaces, the interfaces between two adjacent coarse blocks must lie inside the region over which the local flow is computed. In our coupled local–global upscaling procedure, we consider extended local domains with $r = 0.5$ and

1.5. In order to allow for the calculation of $< p >$ in Eq. (12), only $r = 1.5$ is applied in T^* upscaling.

Permeability upscaling and transmissibility upscaling are two different ways of post-processing (averaging) the local fine scale solutions. In $\mathbf{k}^*$ upscaling, the velocity and pressure gradient in each local fine scale block are first computed, while in T^* upscaling the coarse scale interblock fluxes and averaged pressures in adjacent coarse blocks are calculated. In the context of two-point fluxes, harmonic averaging (Eqs. (5) and (6)) will be applied to obtain T^* from $\mathbf{k}^*$ (with cross terms k^*_{xy} neglected). The use of the harmonic average in this context derives from treating the interblock flows as one-dimensional problems in each of the coordinate directions.

In models with highly discontinuous permeability distributions, such as the channelized systems considered here, the harmonic average of $\mathbf{k}^*$ may introduce considerable approximation error. Specifically, because harmonic averaging puts more weight on smaller values, this procedure can act to underestimate the total flow due to the high contrast between the $\mathbf{k}^*$ in adjacent coarse blocks. Direct transmissibility upscaling (i.e., Eq. (12)), by contrast, avoids the harmonic averaging step and as a result better captures the effects of permeability discontinuities. Therefore, for highly heterogeneous channelized systems, permeability and transmissibility upscalings may provide very different results. Transmissibility upscaling can be expected to be more accurate in terms of reproducing fine scale flow results. This will be illustrated in Section 4 below.

3.3. Iteration between coarse scale global flow and fine scale local flow

In the above sections, we described how to incorporate global coarse pressures into local flow calculations. Specifically, we first perform generic global flows, then solve local flow problems subject to boundary conditions determined from the global flows. The global flow is, however, an approximation obtained using an estimate of coarse properties (e.g., coarse properties from standard upscaling methods). We can improve the global flow approximation through use of the newly calculated coarse properties. This suggests an iterative procedure, in which the goal is consistency between the coarse scale global flow and the fine scale local flows.

The iteration applied here can be viewed as a successive substitution procedure for the solution of a nonlinear coarse scale pressure equation. In standard local or extended local upscaling methods, $\mathbf{k}^*$ or T^* is obtained independent of any global flow problem. In our coupled approach, due to the incorporation of coarse pressures into the local flow problem used to compute $\mathbf{k}^*$ or T^*, Eq. (3) becomes a non-linear equation:

$$\nabla \cdot (\mathbf{k}^*(p^c) \cdot \nabla p^c) = 0, \tag{13}$$

where $\mathbf{k}^*$ is now dependent on p^c (in addition to the local heterogeneity). The five-point discretization form of Eq. (13) for the coarse block (i, j) is written as:

$$(T^*_x)_{i-1/2,j}(p^c_{i-1,j} - p^c_{i,j}) + (T^*_x)_{i+1/2,j}(p^c_{i+1,j} - p^c_{i,j}) + (T^*_y)_{i,j-1/2}(p^c_{i,j-1} - p^c_{i,j}) + (T^*_y)_{i,j+1/2}(p^c_{i,j+1} - p^c_{i,j}) = 0, \tag{14}$$

where T^* depends on coarse pressures p^c in several coarse blocks around the target block where T^* is defined. Note that T^* can be calculated either from the full tensor $\mathbf{k}^*$ (in this case, Eq. (14) is replaced by a corresponding nine-point stencil resulting from a multi-point flux-continuous calculation in [25]), or directly from local flows using Eq. (12).

The solution procedure is illustrated in the flow chart in Fig. 5 (refer also to the schematic of global and local flows in Fig. 3). An initial estimate of coarse properties $\mathbf{k}^*$ or T^* is obtained from standard extended local upscaling, using either constant pressure—no flow or periodic local boundary conditions. Global coarse pressures are then computed using this initial upscaled model. These coarse pressures are in turn interpolated as described above to provide Dirichlet boundary conditions over the extended local region (Eqs. (8) and (9)). The local flow problem (Eq. (1)) is then solved again subject to these pressure boundary conditions and $\mathbf{k}^*$ or T^* (using Eqs. (11) or (12)) is recomputed. With these

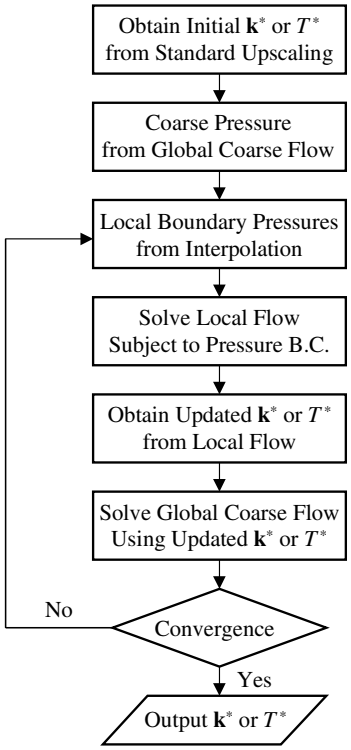

Fig. 5. Flow chart of coupled local–global upscaling approach.

modified $\mathbf{k}^*$ or T^*, we again solve the global coarse flow problem to update the coarse pressures.

Convergence between the local and global flows is checked at each iteration. In our calculations, we define the residual R as

$$R = \frac{\|\delta p_x^c\|_2 + \|\delta p_y^c\|_2}{\|(\delta p_x^c)^1\|_2 + \|(\delta p_y^c)^1\|_2}, \tag{15}$$

where p_x^c and p_y^c designate coarse scale pressures when global flow is in the x and y directions respectively (recall that we have two generic global flows). The sum of the L_2 norms of the absolute change of coarse pressure is normalized by the norms in the first iteration (denominator of Eq. (15)). For a coarse grid of $n_x \times n_y$ blocks, the L_2 norm of the coarse pressure change is calculated via:

$$\|\delta p^c\|_2 = \left[\sum_{i=1}^{n_x}\sum_{j=1}^{n_y}((p_{i,j}^c)^{v+1} - (p_{i,j}^c)^v)^2\right]^{1/2}, \tag{16}$$

where (i,j) is coarse block index and v represents the iteration step. We can also define the residual in terms of changes in the coarse scale velocity or coarse properties (T^* or $\mathbf{k}^*$), though we found that changes in pressure are representative of the other quantities.

We proceed with the iterations until the consistency between the global coarse flow and fine scale local flow is achieved. We refer to this self-consistency as "convergence." The convergence criteria are based on R as well as the change of total flow rate δQ, where

$$\delta Q = \max\left(\frac{|Q_x^{v+1} - Q_x^v|}{|Q_x^0|}, \frac{|Q_y^{v+1} - Q_y^v|}{|Q_y^0|}\right), \tag{17}$$

where Q_x and Q_y are the total flow rate through the system in the x and y directions, which are the coarse scale flow quantities of main interest. The superscript 0 represents the initial estimate of global flow. The iterations are terminated when:

$$R < 0.01 \quad \text{or} \quad \delta Q < 0.001. \tag{18}$$

These tolerances appear reasonable for the problems considered here. Most of the error reduction occurs in the first few iterations, as we will see below.

From the description of the algorithm, we see that the computational cost will essentially be the number of iterations times the cost for the extended local upscaling method. Thus, assuming five iterations are required, the method will cost five times as much as the (non-iterated) extended local procedure. As discussed above, this cost is still often small compared to that of multiple fine scale simulations, which would be required if many flow scenarios and/or two-phase flow simulations are performed.

There are some important differences between our procedure and existing global upscaling methods (e.g., [14]). In most existing global methods, a specific flow scenario is used to obtain the coarse scale T^*. By contrast, our method employs two generic global flows (flows in x and y directions respectively). The resulting coarse properties can therefore be expected to be applicable in more general flow scenarios, especially when combined with near-well upscaling [28]. Using this approach, the occurrence of non-positive coarse properties is significantly reduced relative to some existing procedures (this point will be discussed in detail below). Another potential advantage of our method is that we do not need to solve any global fine scale problems. Rather, we decompose the fine scale global flow solution into a sequence of local flow problems. This approach is preferable when the full global fine scale simulation is prohibitive. The method presented here is also very easily parallelized. This is because the local problems are fully decoupled from each other (even though they are coupled to the coarse scale global flow), so no data exchange is required among the local domains.

3.4. Loss of positivity of $\mathbf{k}^*$ and T^*

The fine scale permeability is required to be a symmetric positive definite tensor. In addition, transmissibility (in a five-point finite difference stencil) should be positive. But, in many upscaling methods, there is no guarantee that the upscaled coarse properties are similarly positive. In global upscaling methods [14], where a specific global flow is applied, an iterative procedure must be applied to eliminate the potentially large number of negative T^*. In purely local upscaling with periodicity, $\mathbf{k}^*$ is guaranteed to be symmetric positive definite [6,7,24]. In extended local methods, however, even periodicity cannot guarantee positive definiteness because of the use of border regions [12]. In such cases, the occurrence of non-positive definiteness is much less frequent than in some global upscaling procedures, since two flows (in the x and y directions respectively) are applied to determine coarse scale parameters. In our method, because we apply two sets of generic global boundary conditions, which result in local flows that are nominally in the x and y directions, the occurrence of negative T^* is greatly reduced compared to global upscaling procedures in which only one global flow is specified.

This can be illustrated by a simple numerical experiment. For a channelized permeability distribution (shown below in Fig. 8a), when we apply one global flow in the x-direction and use the resulting flow to calculate T_x^* and T_y^*, 25 negative T_y^* are obtained out of a total of 110 calculated T_y^* (about 23%). All T_x^* computed from the global solution were positive. In this case, the global flow is in the x-direction and the main channel direction is also in x. If we use global flow in x to calculate T_x^* and global flow in y for T_y^*, the number of negative T_y^* is

reduced to 5. For a simple layered system characterized by two-point geostatistics, the use of two sets of generic global boundary conditions provides T^* that are all positive, whereas the use of global flow in x to compute T_y^* gives about 15% negative T_y^*. This and other examples we have investigated show that negative T^* often occur in low flow regions, and as a result may not have much impact on the total flow through the system.

In our current coupled local–global method, in the few cases when a negative T^* was computed, we replaced it by the T^* calculated using the harmonic average of the appropriate components of $\mathbf{k}^*$ (itself computed from purely local upscaling with periodicity, as in [12]). In general, the occurrence of non-positivity in upscaled properties is a complicated issue that requires additional investigation before more quantitative conclusions can be drawn.

3.5. Reconstruction of subgrid velocity and solution of transport equation

So far we have described the development of a coupled local–global upscaling approach for the solution of the coarse scale flow equation. As indicated earlier, rather than solve a coarse scale transport equation, we reconstruct the fine scale velocity field using the coarse velocity and the subgrid permeability and then solve the fine scale transport equation directly. This equation (Eq. (2)) is solved by integrating along streamlines determined from the reconstructed fine scale velocity.

We could attempt to compute fine scale velocity directly from each local flow problem. The velocity field reconstructed in this way does not satisfy fine scale mass conservation. To circumvent this problem, a purely local region (shown in Fig. 1b) is used for the velocity reconstruction. Neumann boundary conditions as in [17] are applied for this procedure. For a particular coarse block, flux boundary conditions are assigned on all of the fine grid boundary edges that comprise the coarse block edges. The boundary fluxes are apportioned proportional to the fine scale interblock transmissibility. With reference to Fig. 1a and b, for a given coarse block containing $n_x \times n_y$ fine grid cells with fine scale block index (i, j), coarse fluxes q_x^c and q_y^c are obtained from the global coarse scale simulation. We then reapportion the coarse flux on the local fine scale boundaries to obtain the fine scale fluxes. Specifically, for edges along the local boundary $x = 0$,

$$(q_x)_{0,j} = \frac{(T_x)_{1/2,j}}{\sum_{j=1}^{n_y} (T_x)_{1/2,j}} q_x^c, \quad j = 1, \ldots, n_y, \tag{19}$$

where $(q_x)_{0,j}$ represents fine scale flux at the boundary and T_x is the fine scale interblock transmissibility. Fine scale fluxes at other local boundaries are calculated similarly. This reconstruction guarantees flux continuity across fine scale cells in neighboring coarse blocks and accounts for subgrid heterogeneity, in addition to forcing the sum of the fine grid fluxes to be equal to the corresponding coarse grid flux. Subject to the above local boundary conditions, we solve Eq. (1) (pressure is specified at one point to render the problem well-posed) to reconstruct fine scale velocity $\mathbf{u}$.

For the solution of the saturation equation (2), we use the particle tracking procedure described in [26]. From the reconstructed fine scale $\mathbf{u}$, streamlines can be formed and the particles are tracked along streamlines. The flow rate of produced oil (displaced fluid) at the outlet boundary is designated q_o and the flow rate of produced water (displacing fluid) q_w. Note that we consider the transport problem with unit mobility ratio, so oil and water have identical fluid properties and saturation changes will not affect pressure or velocity. We calculate oil cut F_o ($F_o = q_o/q_t$, where $q_t = q_o + q_w$) versus pore volume injected or PVI (dimensionless time). For a system at constant flow rate (as is the case for the unit mobility ratio displacements considered here), $\mathrm{PVI} = q_t t/V_p$, where t is dimensional time and V_p is the total pore volume of the system. The oil cut of the displaced fluid at the outlet F_o is computed by:

$$F_o(t) = 1 - f_b(t), \tag{20}$$

where $f_b(t)$ is the fraction of streamlines that have broken through at time t. The breakthrough time for each streamline is determined via:

$$t_b = \int_l \frac{\mathrm{d}l}{u}, \tag{21}$$

where l is the path along the streamline from the inlet to the outlet and $u = |\mathbf{u}|$. Since the transport equation considered here (Eq. (2)) is for a passive scalar, the (reconstructed) velocity field need only be computed once and need not be updated in time.

In the next two sections, we present results for total flow rate and transport using both standard (extended local) and the coupled local–global upscaling procedures to demonstrate the capabilities of the new method.

4. Flow results using the coupled local–global upscaling approach

The coupled upscaling procedure was applied to several different types of two-dimensional permeability fields. In layered systems with permeability described in terms of a spherical or exponential variogram with correlation lengths in the x and y directions specified, standard methods performed quite well (e.g., errors of $\leqslant 10\%$). In these cases, the improvement achieved by the coupled approach might only be a few percent. In more highly heterogeneous systems, by contrast, the errors using standard methods are larger and the improve-

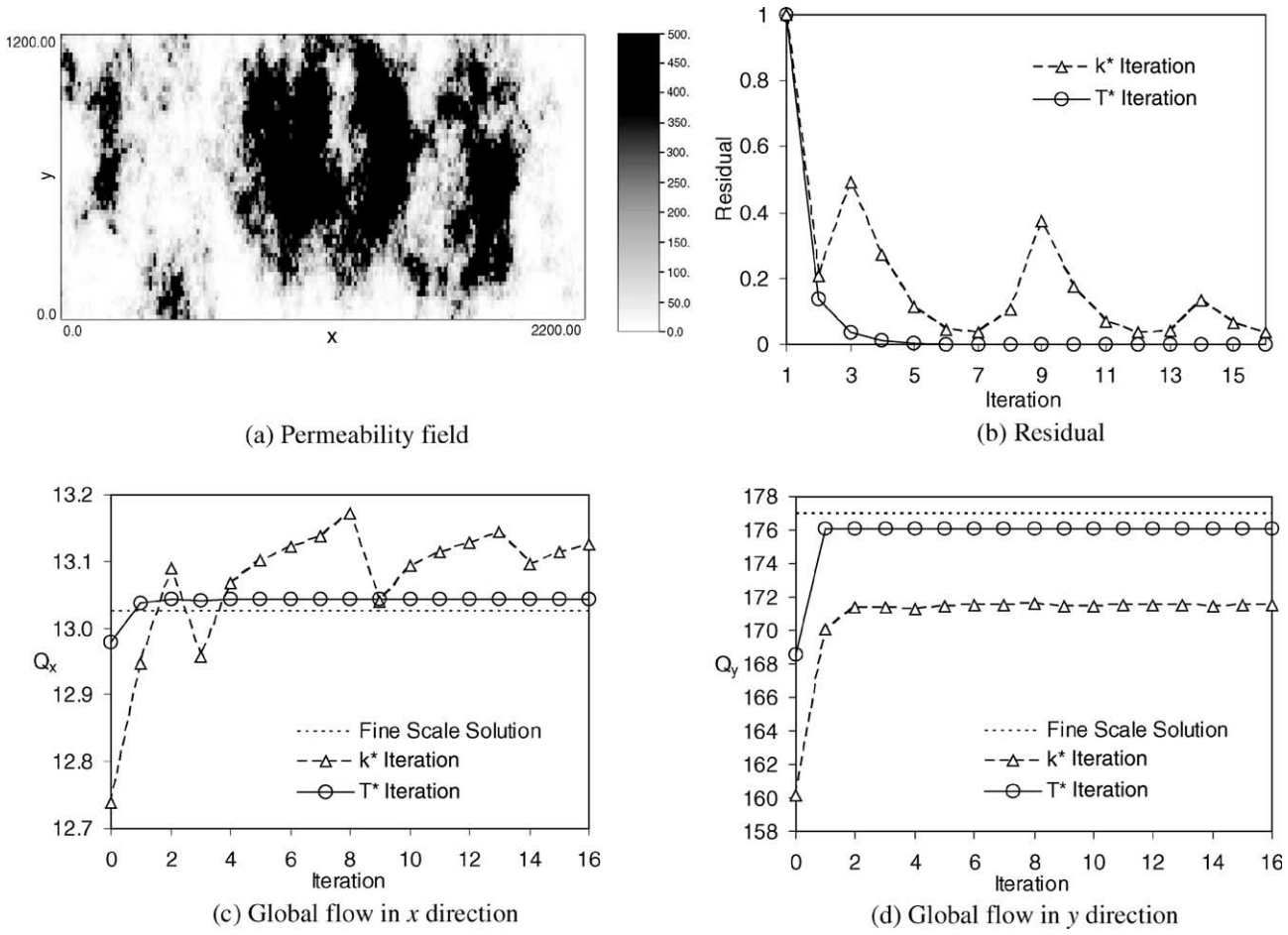

Fig. 6. Permeability field and results for local–global approach with $\mathbf{k}^*$ and T^* upscalings (layer 9 from [29]).

ments offered by the local–global procedure are more substantial.

We therefore present results only for systems with high degrees of heterogeneity. Our models involve channelized subsurface systems and typically display very high variations in permeability over short ranges. They additionally contain geometrically complex features that introduce complicated connectivity into the model. The particular permeability fields are from the North Sea reservoir model applied in [29]. This three-dimensional model includes a total of 85 layers (in the x–y plane), with the 35 upper layers representing a more continuous geology and the 50 lower layers representing highly channelized systems. The very high and abrupt contrast in permeability makes it difficult for standard upscaling methods to provide results of high accuracy.

4.1. General performance of the coupled local–global method

The first system considered is shown in Fig. 6a (this is layer 9 from the model in [29]). This layer is from the more continuous region of the model and is of a complexity between that of layered and channelized systems. Permeability in this model varies by over five orders of magnitude, from a minimum of 0.08 md to a maximum of 20,000 md (the permeability scale in Fig. 6a does not cover this full range). We upscale the fine model, of dimensions 220×60, to a coarse model of dimensions 22×6 using the coupled approach. We set $r = 1.5$ in the local calculation of $\mathbf{k}^*$ and T^*. Global flow in x is driven by prescribing $p = 1$ at the left boundary and $p = 0$ at the right boundary with no flow at the other two boundaries. Flow in y is prescribed analogously. Shown in Fig. 6b is the residual as a function of iteration for both T^* and $\mathbf{k}^*$ upscalings, where the residual is calculated using Eq. (15). Based on the convergence criteria defined in Eq. (18), it takes 16 iterations for $\mathbf{k}^*$ upscaling to converge, while for T^* upscaling, only three iterations are required (in Fig. 6, T^* upscaling results for 16 iterations are displayed). Faster convergence using T^* upscaling was observed in the great majority of cases.

Fig. 6c and d display results for total flow rate through the system (Q_x and Q_y) in the x and y directions respectively. The solid curves and circles represent T^* upscaling; the dashed curves and triangles represent $\mathbf{k}^*$

upscaling. The fine grid solution is indicated by the dotted line. For both Q_x and Q_y, T^* upscaling provides very accurate results—within 1% in both cases (though it is important to note that the initial errors are only about 5%). The use of $\mathbf{k}^*$ upscaling provides less accuracy (see Section 3.2 for further discussion of this point). Due to the higher accuracy and faster convergence of T^* upscaling, in the cases that follow we only present results for this type of upscaling.

Before we present flow results for more complex channelized systems, we first look more closely at the residual for a typical layer. Fig. 7 shows the residual for layer 59 (flow results for this layer will be discussed later) in a semi-log plot. Most error reduction occurs in the first few iterations. After five iterations, R is reduced from 1 to 0.02. At this point, the convergence rate becomes very slow; from iteration 5 to iteration 16, the error is only decreased by 0.01, though a constant convergence rate is observed. This motivates the use of the convergence criteria in Eq. (18), where the iterations will be terminated based on either the total flow rates or R.

We now consider flow results for layer 59, a highly heterogeneous layer from the channelized portion of the model, as shown in Fig. 8a. Here, the permeability can be seen to vary by several orders of magnitude over short distances (the permeability varies by seven orders of magnitude in this model). In addition, the interconnected channels provide complex large scale connectivity which strongly impacts flow. In this case, the initial errors using T^* upscaling are considerably higher than in the previous case—15% (in Q_x) and 25% (in Q_y). After local–global iteration, the coarse model flow rates are very close to the fine grid solutions. Specifically, the error in Q_x is reduced to 5.7% (Fig. 8b) and that in Q_y is reduced to 0.5% (Fig. 8c). After four iterations, R is reduced to 0.024, as shown in Fig. 7, and Q_x and Q_y are stabilized (for the tolerance given in Eq. (18)).

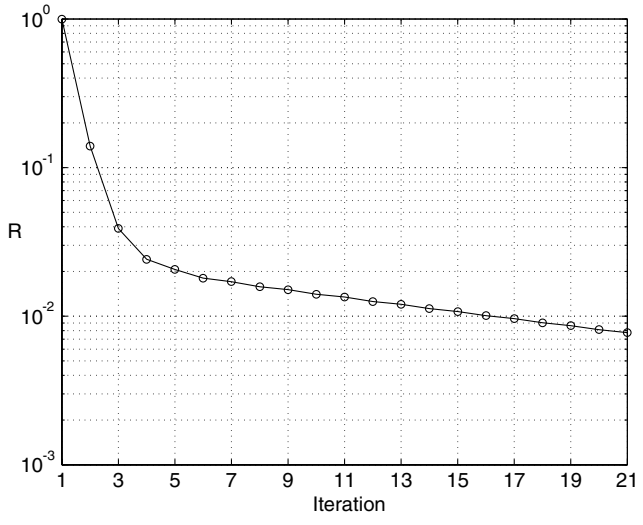

Fig. 7. Semi-log plot of the residual for coupled local–global T^* upscaling (layer 59).

Figs. 9 and 10 show total flow results for two other layers. Coarse scale models of these layers generated using standard techniques display very significant errors in total flow rate. For layer 48 (Fig. 9), the fine scale Q_x is 5.59. Using the initial estimate for T^* (computed, as in the previous cases, using extended local T^* upscaling with $r = 1.5$ and periodic boundary conditions) gives $Q_x = 2.08$, an error of 63%. Our coupled procedure gives $Q_x = 5.02$, reducing the error to 10%. Similarly, for layer 47 (Fig. 10), the initial Q_y of 2.88 displays an error of 73%. This is improved after iteration to 9.6, an error of 10% compared to the fine solution of 10.6. These two extreme examples demonstrate that, for highly heterogeneous formations, existing upscaling methods (even using border regions and direct T^* calculation) may not provide satisfactory results. We note that other boundary conditions (e.g., pressure—no flow) will perform better in some cases, so the local results could be improved somewhat (see below). The coupled local–global approach, by contrast, performs quite well for these highly heterogeneous systems.

4.2. Effects of initial T^* and upscaling ratio

We now perform some sensitivity studies to illustrate the robustness of our coupled local–global upscaling method. We discuss the effects of the initial T^* estimates and upscaling ratio on the performance of the method.

The initial T^* can be obtained using different local boundary conditions and with border regions of varying size. The effects of these specifications are shown in Fig. 11 (these results are for layer 59). In the previous examples we computed the initial T^* using $r = 1.5$ and periodic boundary conditions. Using a slightly smaller local region ($r = 1$), a less accurate initial estimate for Q_y is obtained. Specifically, the error in Q_y in this case is 50%, as indicated in Fig. 11. Even using this inaccurate initial estimate for T^*, the coupled procedure closely approaches the fine scale solution after only five iterations. Setting the initial local boundary condition to constant pressure—no flow provides a more accurate initial estimate for Q_y. This may be because the specification of periodicity acts to disrupt critical large scale high flow pathways in the permeability field, which the pressure—no flow specification maintains to a greater degree. In any event, the iterative procedure again drives the solution very close to the fine grid solution after a few iterations. We emphasize that the coupled procedure, even using the least accurate initial T^* estimate, provides results that are superior to those from any of the extended local upscaling techniques used for the initial estimates in Fig. 11.

We next present results using different upscaling ratios (again for layer 59). Flow results for coarse models

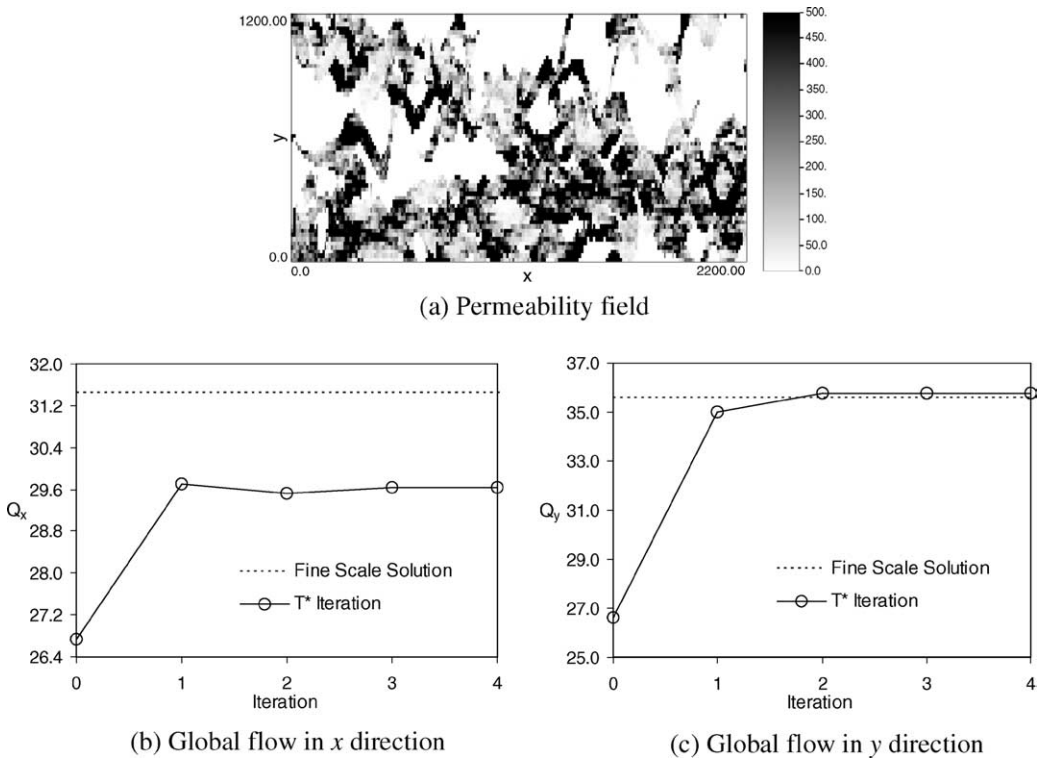

(a) Permeability field

(b) Global flow in x direction

(c) Global flow in y direction

Fig. 8. Permeability field and results for local–global T^* upscaling (layer 59).

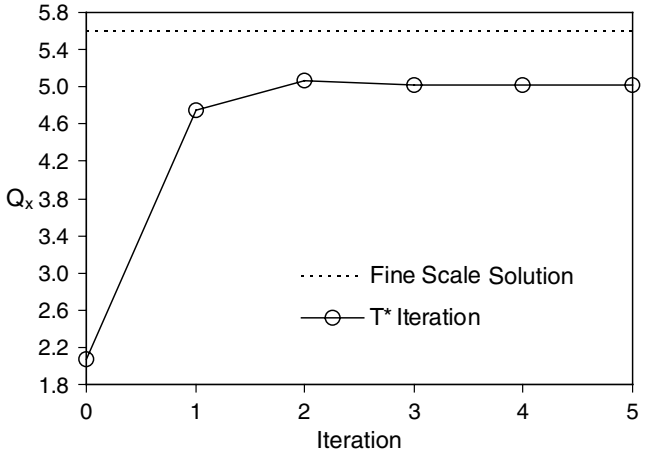

Fig. 9. Flow results for Q_x for layer 48 (error is reduced from 63% to 10%).

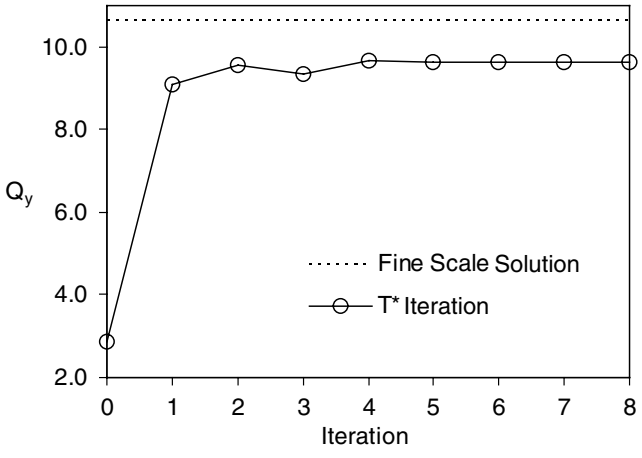

Fig. 10. Flow results for Q_y for layer 47 (error is reduced from 73% to 10%).

of dimensions 22×6, 22×15 and 44×20 (upscaling ratios of 100, 40 and 15 respectively) are presented in Fig. 12. Significant differences are observed in the initial flow rates, though these differences are reduced considerably after iterating. Some differences do persist, however, with the most accurate upscaled results corresponding to the coarsest model. This is likely because the various models have border regions of quite different sizes; i.e., a specification of $r = 1.5$ means that the coarsest model contains the largest border region.

4.3. Results for channelized systems

We now apply the local–global upscaling technique to all of the 50 channelized layers from the model in [29]. The coarse models are in all cases 22×6. Based on the convergence criteria of Eq. (18), of the 50 layers there are 24 layers for which it takes five or fewer iterations to obtain converged results. There are 12 layers in which converged solutions are not achieved after 30 iterations. Oscillations with an average magnitude of ±2% in the

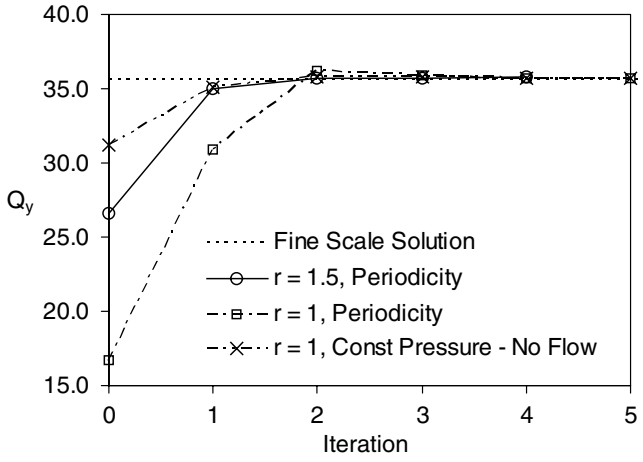

Fig. 11. Effects of initial estimates for T^* on local–global upscaling results (layer 59).

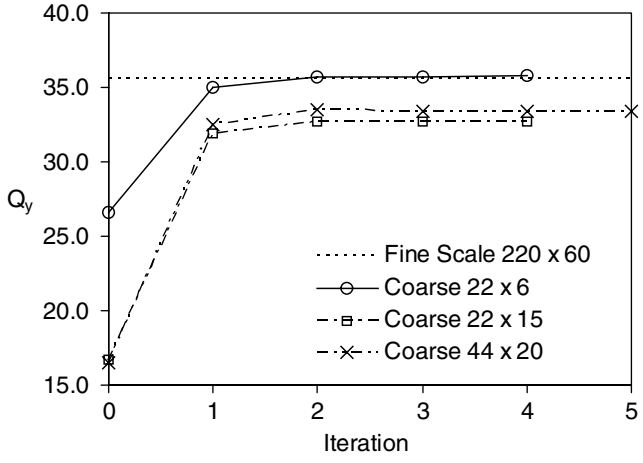

Fig. 12. Effects of upscaling ratio on local–global upscaling results (layer 59).

total flow rate are observed in these layers. However, the errors in Q_x and Q_y are in all cases reduced from their initial values through iteration. Specifically, for the 12 layers that do not converge, the average error in Q_x is reduced from 28.7% to 13.4% and that in Q_y is decreased from 23.2% to 9.1%. Again, most error reduction occurs in the first few iterations. For the more continuous portions of the three-dimensional model from [29] (layers 1–35), converged solutions were obtained within five iterations in all cases when T^* upscaling was used. For highly heterogeneous channelized systems, our method cannot guarantee convergence (according to the criteria in Eq. (18)), but it still provides improved coarse models in all cases. From a practical point of view, therefore, we will generally expect to use only a few iterations to obtain improved coarse properties.

Scatter plots comparing the Q_y computed in the fine scale models with those computed from the coarse

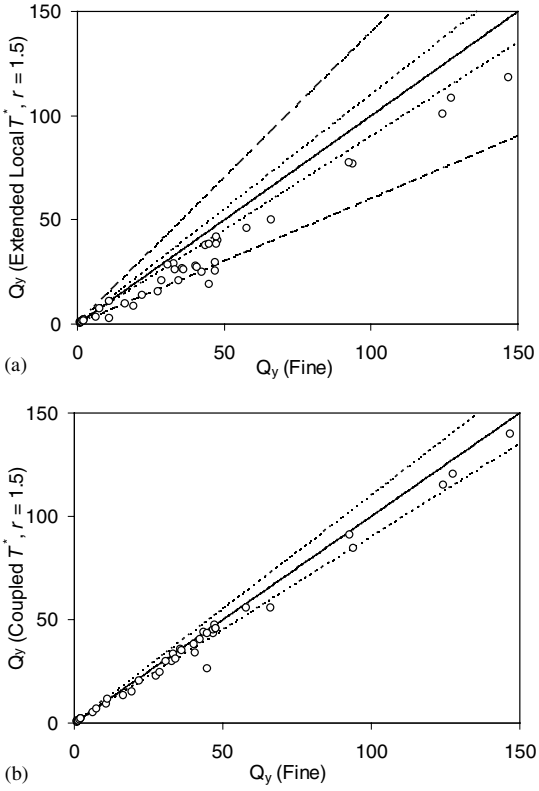

Fig. 13. Comparison of fine and coarse scale flow results with (a) extended local upscaling and (b) coupled local–global upscaling for channelized systems (layers 36–85).

models are presented in Fig. 13. We compare the results using the locally calculated T^* (with $r = 1.5$ and periodic boundary conditions) against the fine scale results in Fig. 13a and results using local–global upscaling against the fine scale results in Fig. 13b. In these calculations, only five iterations on T^* were performed. The dotted and dashed lines in Fig. 13a and b indicate ±10% and ±40% errors, respectively. It is evident from the plots that the coarse scale results using the local–global approach are more accurate overall than those using the extended local technique. The mean error in Fig. 13a is 21%; it is reduced to less than 7% in Fig. 13b. In addition, it is apparent from the figures that many of the systems with the largest errors in Fig. 13a are modeled with reasonable accuracy in Fig. 13b.

4.4. Estimated fine scale pressure field

In order to understand why the coupled method provides accurate coarse models, we look briefly at the pressure fields used in the calculation of T^*. We can extract pressures from the local flow calculations and assemble them to obtain an estimate of the global fine scale pressure distribution. Contours of pressure computed in this way are presented in Fig. 14a and b. These pressure fields correspond to the first iteration and

converged solutions. The pressure distribution obtained from the global fine scale simulation is shown in Fig. 14c. Comparison of these pressure fields shows that the reassembled local approximations are quite close to the global solution, even in the first iteration. An approximation of this level of accuracy cannot be achieved from a local or extended local calculation with the assumption of constant pressure difference. We note that previous researchers have also reconstructed fine scale pressures from local flows [19]. However, in that study, only geometric means were used to compute coarse properties and no iterations were performed.

4.5. Application for two-phase flow

We now illustrate how coarse properties (T^*) derived from single-phase flow calculations can be used for a two-phase flow problem. For a two-phase flow system, the pressure equation (1) becomes

$$\nabla \cdot (\mathbf{k}\lambda(S) \cdot \nabla p) = 0, \tag{22}$$

where $\lambda(S)$ is the total mobility, defined as $\lambda(S) = k_{rw}(S)/\mu_w + k_{ro}(S)/\mu_o$, with k_{rw} and k_{ro} the relative permeabilities to the water and oil phases. In the saturation equation (2), $\mathbf{u}S$ is replaced by $\mathbf{u}f(S)$, where $\mathbf{u}$ is the total Darcy velocity and $f(S)$ is the Buckley–Leverett fractional flow function determined from the relative permeabilities. For two-phase flow, the total mobility $\lambda(S)$ varies with time due to the dependency on saturation. Therefore, the pressure field and total velocity change at each time step.

We consider a two-phase flow with $k_{rw} = S^2$, $k_{ro} = (1-S)^2$ and $\mu_o/\mu_w = 10$, where μ_o and μ_w are the oil and water viscosities. This corresponds to a mobility ratio of 10. We consider layer 59 (shown in Fig. 8a), and specify global flow in the y-direction. Water is injected from the lower boundary, with the system initially saturated with oil. A fully implicit finite difference procedure is applied to solve the pressure and saturation equations on both the fine and coarse scales. The fine scale model is of dimensions 220×60 and the coarse model is 22×6. No two-phase upscaling was performed on the coarse model.

Fig. 15 shows the total liquid (oil plus water) flow rate (q_t is here normalized by the initial total flow rate of the fine scale solution) versus PVI for the fine scale model (solid line), the coarse scale model using the coupled local–global T^* (dotted line), and the coarse scale model using the extended local T^* (dashed line). In this case, because q_t varies in time, PVI is given by $\frac{1}{V_p}\int_0^t q_t \,d\tau$. At the early stage of water injection, the coupled local–global T^* provides equivalent accuracy as in single-phase flow. The simulation using the extended local T^*, by contrast, underestimates the total flow rate, as was observed for single-phase flow. This clearly demonstrates

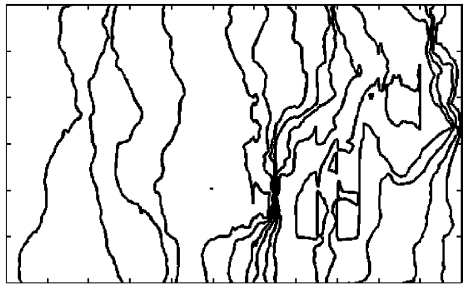

(a) Pressure in first iteration

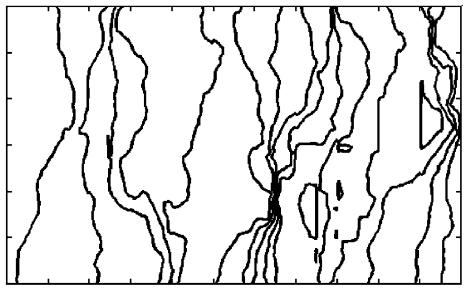

(b) Pressure in converged solution

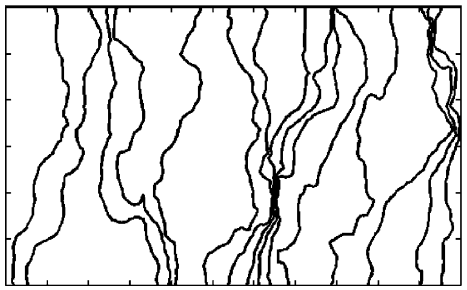

(c) Fine scale pressure

Fig. 14. Comparison of pressure contours assembled from (a and b) coupled local–global method and (c) fine scale solution (layer 59).

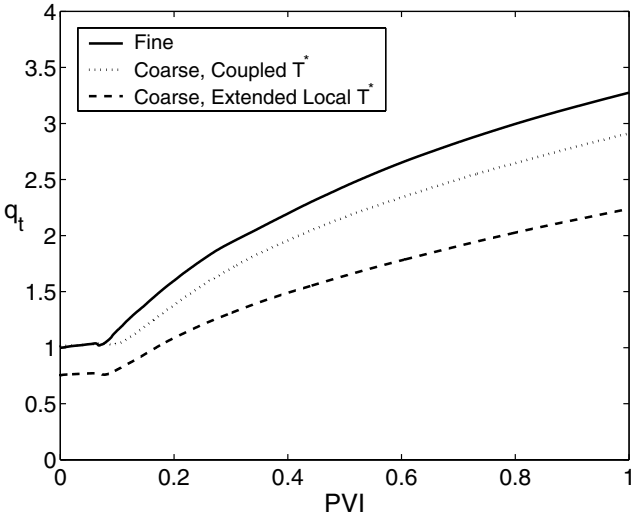

Fig. 15. Total flow rate of two-phase flow (layer 59).

that accurate single-phase coarse properties are important for achieving accurate two-phase flow results. At later times there are larger differences in total flow rate between the fine and coarse scale results. At $t = 1$ PVI, the error using the extended local T^* is 32%, while that for the coupled local–global T^* is 11%. The error in the coupled local–global simulation could be reduced through use of two-phase upscaling techniques (see e.g., [27] and references therein). We reiterate that an essential component in two-phase upscaling is an accurate single-phase upscaling, as is provided by our coupled local–global procedure.

It is of interest to consider the computational requirements for the fine and coarse scale simulations. For each time step, the CPU time for the coarse model (22×6) is only about 0.5% of that for the fine scale model (220×60). In practice, larger time steps may be applied to the coarse model, which will further reduce the computational expenses. The overhead of generating the coarse scale properties, which is accomplished in a pre-processing step, is small compared to the computational requirements of the simulation run. This demonstrates the significant savings that can be achieved using upscaling procedures.

5. Transport results using reconstruction of subgrid velocity

We now present results for transport of unit mobility ratio using the subgrid velocity reconstruction and streamline tracing, which are described in Section 3.5. We consider the system to be initially saturated with an oil component and inject water at the left boundary. Unless otherwise specified, we fix $p = 1$, $S = 1$ at the left boundary, $p = 0$ at the right boundary, and no-flow at the remaining boundaries. Because the system is of unit mobility ratio, the velocity field does not change in time. Results are presented in terms of oil cut, F_o, versus pore volume injected, PVI.

5.1. Purely layered systems

To illustrate the potential usefulness of velocity reconstruction, we first consider an idealized case involving a completely layered system. The fine scale system is 20×20 and the coarse system is 5×5. Because the system is completely layered, exact upscaling (in terms of total flow rate) can be accomplished analytically or with a purely local upscaling procedure. Transport results in terms of F_o versus PVI are shown in Fig. 16. The fine result is represented by the solid line, the coarse result computed directly on the coarse grid (no subgrid velocity reconstruction) by the dashed line and the coarse scale result using subgrid velocity reconstruction by the points. The standard coarse grid result displays very large errors and overpredicts breakthrough time (the time when water appears at the outlet) by over a factor of three. The coarse model using velocity reconstruction, by contrast, agrees exactly with the fine model. This is because, for completely layered systems, the flux through any fine grid cell is exactly proportional to the fine grid transmissibility, so the reconstruction is exact. Both coarse models provide the exact total flow rate for this problem. This case, though highly idealized, demonstrates that the use of reconstructed subgrid velocity information can greatly improve transport predictions.

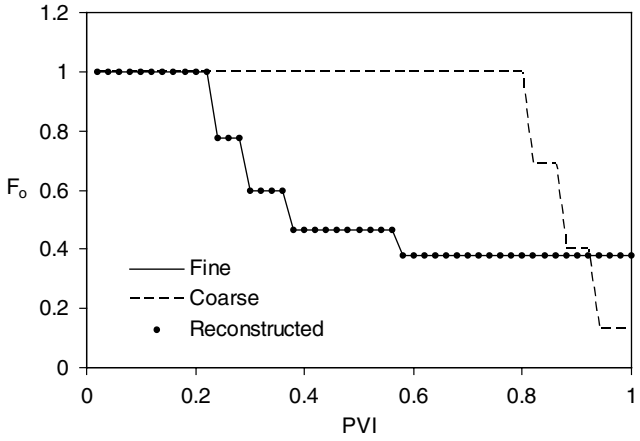

Fig. 16. Oil cut at production edge for exactly layered system.

5.2. Channelized systems

We next turn to the complex channel system from [29] to illustrate the velocity reconstruction coupled with the local–global scale up approach. Fig. 17 shows oil cut computed using subgrid velocity reconstruction with locally calculated T^* (Fig. 17a) and that computed using subgrid velocity reconstruction with T^* from the local–global procedure (Fig. 17b) for layer 59. Compared to the standard coarse models, velocity reconstruction clearly improves the transport predictions. Reconstructed results with the coupled T^* are slightly better than those with the extended local T^*, though the improvement is not dramatic.

We next consider layer 37. For the fine grid model, the total flow is $Q_x = 1.86$ in this case. For the local coarse model we obtain $Q_x = 0.53$ (error of 72%) while for the coupled local–global upscaled model $Q_x = 1.50$ (error of 19%). Similar improvements are observed in transport calculations for this system, as shown in Fig. 18. The large errors evident in Fig. 18a using the locally calculated T^* (with velocity reconstruction) are reduced significantly in Fig. 18b, where T^* is computed from the local–global procedure. This result is also much more accurate than the coarse result without velocity reconstruction.

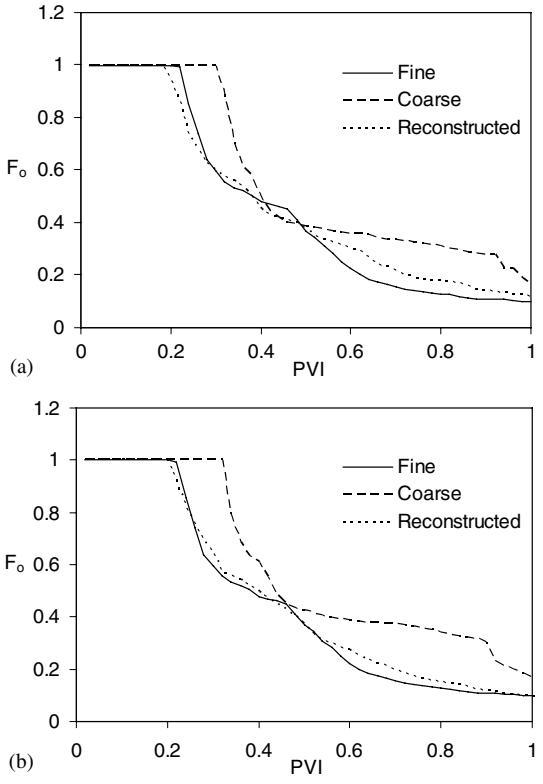

Fig. 17. Oil cut at production edge for channel system using (a) extended local T^* and (b) T^* from coupled local–global procedure (layer 59).

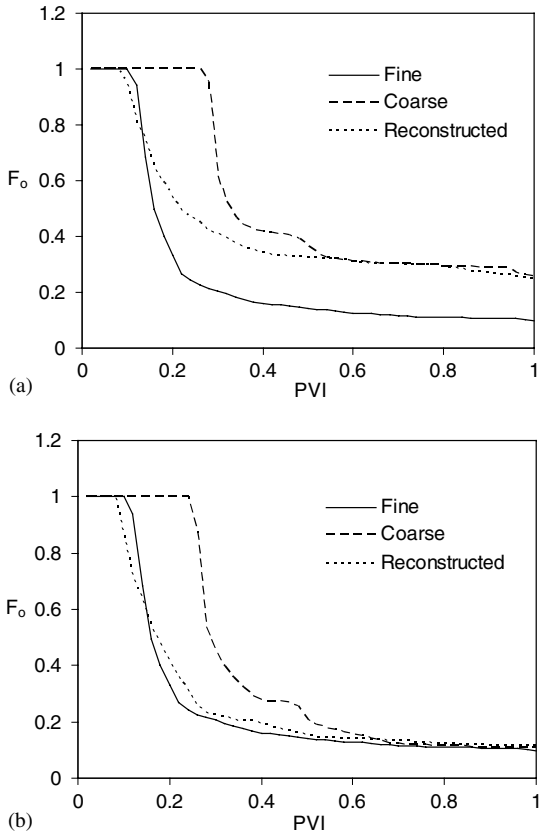

Fig. 18. Oil cut at production edge for channel system using (a) extended local T^* and (b) T^* from coupled local–global procedure (layer 37).

The water saturation distributions shown in Fig. 19 provide a more detailed comparison of fluid transport. Fig. 19a–c show saturations at 0.8 PVI for layer 37 for (a) the reference fine scale solution, (b) the coarse solution using extended local T^* with velocity reconstruction and (c) the coarse solution using the local–global T^* with velocity reconstruction. The saturations in Fig. 19c are clearly in better agreement with the fine scale results than are the saturations in Fig. 19b, again demonstrating the improvement offered by the local–global upscaling approach.

Our last example demonstrates the potential applicability of the upscaled model for flow and transport driven by more general global boundary conditions. In our coupled local–global approach for the calculation of T^*, the global coarse flows involve flow from left to right and flow from bottom to top (which we refer to as "generic global flows"). We now apply the T^* generated from this procedure to other global flows. Using layer 37, flow from the lower right corner to the upper left corner (specifically, $p = 1$ for $0.5L_x \leqslant x \leqslant L_x$, $y = 0$; $p = 0$ for $0 \leqslant x \leqslant 0.5L_x$, $y = L_y$; no flow elsewhere, where L_x and L_y designate the global dimensions) and flow from the lower left corner to the upper right corner ($p = 1$ for $0 \leqslant y \leqslant 0.5L_y$, $x = 0$; $p = 0$ for $0.5L_y \leqslant y \leqslant L_y$, $x = L_x$; no flow elsewhere) are considered. Oil cut curves for these cases are presented in Fig. 20a and b. Close agreement between the reconstructed coarse grid results and the fine scale simulations is achieved in both cases. The total flow rate for the fine scale system in Fig. 20a is 0.284, while that for the coarse solution is 0.263. For the case shown in Fig. 20b, the fine and coarse flow rates are 1.79 and 1.36. The level of accuracy of these results is comparable to that achieved in the side to side generic global flows considered above. This suggests that our coupled local–global upscaling procedure can provide results of reasonable accuracy for large scale flows that somewhat resemble the generic flows used to compute the T^*.

In practice, many flows are driven by wells, and for this type of problem, near-well upscaling techniques (e.g., [28]) must be applied. The introduction of wells may additionally change global flow significantly and the coarse properties generated from the two generic global flows might lose accuracy in some cases. For such problems, the T^* can be recomputed, based on the actual well configuration and flow rates, using a local–global procedure analogous to that applied here. The overall issue of robustness with respect to global boundary conditions is complex and will be addressed in detail in a future paper. The coupled local–global upscaling technique presented here is, however, well

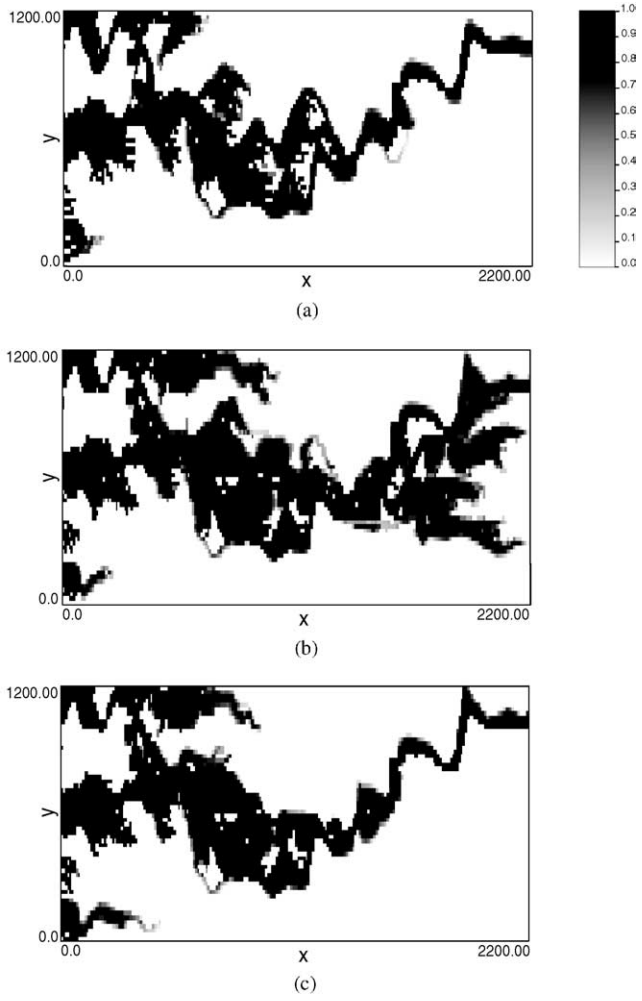

Fig. 19. Water saturation at $t = 0.8$ PVI for channel system (layer 37): (a) water saturation from fine scale solution, (b) water saturation from reconstruction using extended local T^* and (c) water saturation from reconstruction using coupled local–global T^*.

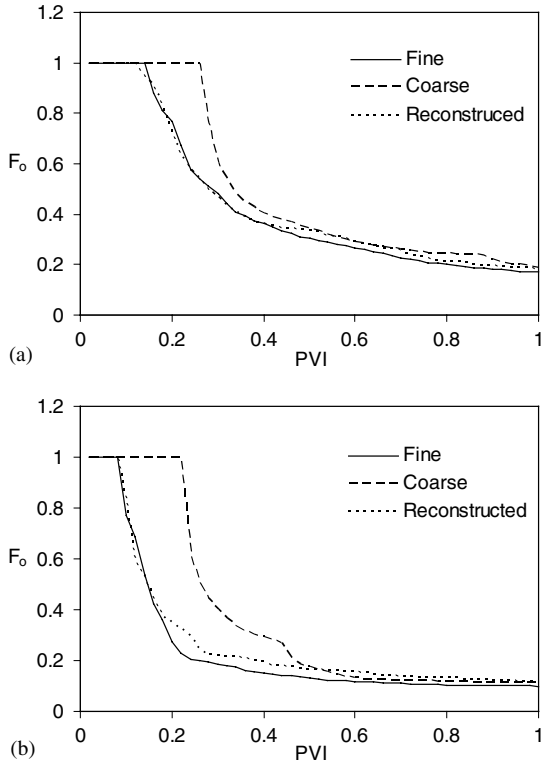

Fig. 20. Oil cut at production edge for channel system for different global boundary conditions (layer 37): (a) oil cut for flow from lower right corner to upper left corner and (b) oil cut for flow from lower left corner to upper right corner.

suited to accommodate the effects of general global flows on coarse properties.

6. Discussion

In this paper, we presented a new coupled local–global upscaling approach. The method uses coarse pressures from generic global flows to determine the local boundary conditions used for the calculation of upscaled transmissibility (T^*) or permeability ($\mathbf{k}^*$). As a result, both the large scale flow and the subgrid permeabilities impact the upscaled parameters. The method does not require any global fine scale calculations and is well suited for parallelization. Solution stabilization in terms of total flow is generally achieved after the first few iterations, so computational requirements are not excessive compared to existing extended local upscaling techniques.

Numerical experiments using the new method demonstrated significantly improved coarse scale results for total flow relative to those obtained using standard upscaling techniques. This is due in part to the potential inaccuracy of the standard assumption of constant local pressure difference for the highly heterogeneous cases considered. The method converged faster and provided more accurate coarse scale results when upscaled transmissibility was computed directly (rather than from $\mathbf{k}^*$). The local–global upscaling method was also shown to be robust with respect to the initial estimate for the upscaled parameters and to the degree of coarsening. The coupled local–global technique could be modified through use of different approaches for determining the local boundary conditions for the upscaling calculation. The current pressure interpolation is quite simple and it is possible that other procedures for the interpolation of the coarse pressure might provide improved performance.

We also applied a subgrid velocity reconstruction technique for use in transport calculations. Our reconstruction approach followed the method presented in [17]. We applied this procedure in conjunction with the coupled local–global upscaling technique and demonstrated improved results relative to the use of velocity reconstruction with locally computed T^*. This indicates

that our upscaling procedure acts to provide enhanced results for both flow and transport. In subsequent work, we plan to couple our local–global upscaling with subgrid models for transport (i.e., an upscaled version of Eq. (2)). This will allow the flow and transport problems to be solved on the same coarse grid.

With any upscaling technique, an important issue is the level of robustness of the coarse model with respect to global boundary conditions or well locations. Our procedure applies two sets of generic global boundary conditions for the calculation of T^* or $\mathbf{k}^*$. In limited tests, it appears that coarse models obtained in this way are suitable in some cases for use with other boundary conditions that resemble the generic global boundary conditions (e.g., results of reasonable accuracy were obtained for some corner to corner flows). Our coupled local–global upscaling method can be extended to adjust the coarse scale T^* or $\mathbf{k}^*$ based on the actual global boundary conditions or well locations. It can also be readily applied in combination with near-well upscaling approaches (e.g., [28]). It may also be useful to combine the method with flow-based grid generation procedures [11,30] so some aspects of the fine scale permeability field are resolved explicitly. Several of these extensions will be explored in future work.

7. Conclusions

The following main conclusions can be drawn from this study:

- A new coupled local–global upscaling approach was developed and applied. The method does not require any global fine scale calculations. Instead, the technique uses generic global coarse scale flow computations to determine the local boundary conditions for use in the calculation of upscaled permeability or transmissibility. Iterations are performed in order to achieve consistency between the upscaled parameters and the global pressure field.
- For highly heterogeneous channelized systems, it was found that the direct upscaling of transmissibility using the coupled approach provided more accurate coarse scale results than permeability upscaling. In addition, fewer iterations were generally required in transmissibility upscaling.
- The coarse models obtained from the new method provide considerably more accurate simulation results than do models developed using existing local procedures. In some cases coarse models generated using existing techniques predicted global flow quantities with errors of 50% or greater. For these systems the coupled local–global approach provided coarse models that predict global flow to within about 10%. In limited tests, coarse models developed using the new coupled technique were found to be appropriate for other global boundary conditions, suggesting that at least for some permeability distributions the method is reasonably robust.
- Transport calculations were performed using a subgrid velocity reconstruction procedure. It was demonstrated that better accuracy was achieved in these results when the velocity reconstruction was used in conjunction with the coupled local–global upscaling method.

Acknowledgements

This work was funded in part by the industrial affiliates of the Stanford University Reservoir Simulation Research Project (SUPRI-B) and by the US Department of Energy under contract number DE-AC26-99BC15213.

References

[1] Wen XH, Gómez-Hernández JJ. Upscaling hydraulic conductivities in heterogeneous media: an overview. J Hydrol 1996;183:ix–xxxii.
[2] Renard P, de Marsily G. Calculating effective permeability: a review. Adv Water Resour 1997;20:253–78.
[3] Farmer CL. Upscaling: a review. Int J Numer Meth Fluids 2002;40:63–78.
[4] Scheibe T, Yabusali S. Scaling of flow and transport behavior in heterogeneous groundwater systems. Adv Water Resour 1998;22:223–38.
[5] Pickup GE, Ringrose PS, Jensen JL, Sorbie KS. Permeability tensors for sedimentary structures. Math Geol 1994;26:227–50.
[6] Kitanidis PK. Effective hydraulic conductivity for gradually varying flow. Water Resour Res 1990;26:1197–208.
[7] Durlofsky LJ. Numerical calculation of equivalent grid block permeability tensors for heterogeneous porous media. Water Resour Res 1991;27:699–708.
[8] Holden L, Lia O. A tensor estimator for the homogenization of absolute permeability. Transport Porous Med 1992;8:37–46.
[9] Gómez-Hernández JJ, Journel AG. Stochastic characterization of grid block permeability. SPE Format Evaluat 1994;9:93–9.
[10] Wu XH, Efendiev YR, Hou TY. Analysis of upscaling absolute permeability. Discrete Contin Dyn Systems, Series B 2002;2:185–204.
[11] Wen XH, Durlofsky LJ, Edwards MG. Upscaling of channel systems in two dimensions using flow-based grids. Transport Porous Med 2003;51:343–66.
[12] Wen XH, Durlofsky LJ, Edwards MG. Use of border regions for improved permeability upscaling, Math Geol, in press.
[13] White CD, Horne RN. Computing absolute transmissibility in the presence of fine-scale heterogeneity, Paper SPE 16011 presented at the SPE Symposium on Reservoir Simulation, San Antonio, TX, 1–4 February 1987.
[14] Holden L, Nielsen BF. Global upscaling of permeability in heterogeneous reservoirs: the Output Least Squares (OLS) method. Transport Porous Med 2000;40:115–43.
[15] Lunati I, Bernard D, Giudici M, Parravicini G, Ponzini G. A numerical comparison between two upscaling techniques:

non-local inverse based scaling and simplified renormalization. Adv Water Resour 2001;24:913–29.
[16] Aarnes JE. On numerical methods for multifield problems and fast reservoir performance prediction, Ph.D. thesis, University of Bergen, Norway, 2002.
[17] Gautier Y, Blunt MJ, Christie MA. Nested gridding and streamline-based simulation for fast reservoir performance prediction. Computat Geosci 1999;3:295–320.
[18] Ramè M, Killough J. A new approach to the simulation of flows in highly heterogeneous porous media, Paper SPE 21247 presented at the SPE Symposium on Reservoir Simulation, Anaheim, CA, 17–20 February 1991.
[19] Guérillot D, Verdière S. Different pressure grids for reservoir simulation in heterogeneous reservoirs, Paper SPE 29148 presented at the SPE Symposium on Reservoir Simulation, San Antonio, TX, 12–15 February 1995.
[20] Moulton DJ, Dendy JE, Hyman JM. The black box multigrid numerical homogenization algorithm. J Computat Phys 1998;142:80–108.
[21] Hou TY, Wu XH. A multiscale finite element method for elliptic problems in composite materials and porous media. J Computat Phys 1997;134:169–89.
[22] Arbogast T, Bryant SL. A two-scale numerical subgrid technique for waterflood simulations. SPE J 2002;7:446–57.
[23] Jenny P, Lee SH, Tchelepi HA. Multi-scale finite-volume method for elliptic problems in subsurface flow simulation. J Computat Phys 2003;187:47–67.
[24] Bourgeat A. Homogenized behavior of two-phase flows in naturally fractured reservoirs with uniform fractures distribution. Comput Meth Appl Mech Eng 1984;47:205–16.
[25] Lee SH, Durlofsky LJ, Lough MF, Chen WH. Finite difference simulation of geologically complex reservoirs with tensor permeabilities. SPE Reservoir Evaluat Eng 1998;1:567–74.
[26] Durlofsky LJ, Jones RC, Milliken WJ. A nonuniform coarsening approach for the scale up of displacement processes in heterogeneous media. Adv Water Resour 1997;20:335–47.
[27] Wallstrom TC, Hou S, Christie MA, Durlofsky LJ, Sharp DH, Zou Q. Application of effective flux boundary conditions to two-phase upscaling in porous media. Transport Porous Med 2002;46:155–78.
[28] Durlofsky LJ, Milliken WJ, Bernath A. Scaleup in the near-well region. SPE J 2000;5:110–7.
[29] Christie MA, Blunt MJ. Tenth SPE comparative solution project: a comparison of upscaling techniques. SPE Reservoir Evaluat Eng 2001;4:308–17.
[30] Cirpka OA, Frind EO, Helmig R. Streamline-oriented grid generation for transport modelling in two-dimensional domains including wells. Adv Water Resour 1999;22:697–710.